

Trophectoderm mechanics direct epiblast shape upon embryo implantation

Antonia Weberling¹ & Magdalena Zernicka-Goetz^{1,6*}

¹ Mammalian Embryo and Stem Cell Group, University of Cambridge, Department of Physiology, Development and Neuroscience, Downing Street, Cambridge CB2 3DY, UK

² Plasticity and Self-Organization Group, California Institute of Technology, Division of Biology and Biological Engineering, 1200 E. California Boulevard, Pasadena, CA 91125, USA

* **Lead Contact Email:** mz205@cam.ac.uk

Abstract (word limit 150)

Implantation is a hallmark of mammalian embryogenesis during which embryos establish their contacts with the maternal endometrium, remodel, and undertake growth and differentiation. The mechanisms and sequence of events through which embryos change their shape during this transition are largely unexplored. Here, we show that the first extraembryonic lineage, the polar trophoctoderm, is the key regulator for remodelling the embryonic epiblast. Loss of its function following immuno-surgery or inhibitor treatments prevents the epiblast shape transitions. In the mouse, the polar trophoctoderm exerts physical force upon the epiblast causing it to transform from an oval into the cup shape. In human embryos, the polar trophoctoderm behaves in the opposite manner, exerting a stretching force. By mimicking this stretching behaviour in mouse embryogenesis, we could direct the epiblast to adopt the disc-like shape characteristic of human embryos at this stage. Thus, the polar trophoctoderm acts as a conserved regulator of epiblast shape.

Key Words

Epiblast, Trophectoderm, Morphogenesis, Mouse/Human Implantation, Tissue Remodelling.

Introduction

During implantation, the mammalian embryo is comprised of three lineages: the extra-embryonic trophoctoderm (TE) and primitive endoderm and the embryonic epiblast. The TE forms a hollow cyst, enclosing the proximal side of the epiblast with its polar and the blastocoelic cavity with its mural part. In mouse embryos, the epiblast is covered on its distal side by the primitive endoderm, while in human embryos the second lineage segregation has not yet been completed at this stage. In the mouse, implantation takes place at embryonic day (E) 4.5, is mediated by the mural TE and followed by a series of remodelling events that lead to formation of the egg cylinder, a characteristic of rodent embryos (Molè et al., 2020; Smith, 1980). The establishment of a tissue boundary between polar and mural TE leads to the transformation of the polar TE from a squamous to a thick pseudostratified epithelium due to an increased cell proliferation rate and high contractility (Copp, 1978, 1979; Christodoulou et al., 2019). Invagination of the polar TE via apical constriction, pushes the epiblast into the blastocoelic cavity giving rise to the cylindrical morphology of the post-implantation embryo (Christodoulou et al., 2019). Human embryo implantation is mediated by the polar TE instead and its post-implantation morphogenesis diverges drastically from the mouse leading to formation of a bilaminar disc shaped epiblast as opposed to the egg cylinder (Hertig et al., 1956; Molè et al., 2020).

Generation of forces at the cellular level, their integration and propagation across tissues drives tissue morphogenesis is the generation (Heer and Martin, 2017; Martin et al., 2010; Pinheiro and Bellaïche, 2018). For this, forces must first be built up in individual cells through actomyosin networks that generate contractility and thereby tension in the cell cortex (Cartagena-Rivera et al., 2016; Chugh et al., 2017; Svitkina, 2020). The actomyosin-rich cortex is bound to the cell membrane by the α -catenin - β -catenin complex that regulates cytoskeletal organisation through α -catenin - E-Cadherin interactions (Nelson, 2008; Yamada et al., 2005). E-Cadherin forms adherens junctions and allows propagation of tension throughout a tissue. Increased tension results in the growth and stabilisation of the junctions to ensure tissue integrity. Thus, E-Cadherin serves as a mechano-sensor (Buckley et al., 2014; Le Duc et al., 2010; Martin et al., 2010; Pinheiro and Bellaïche, 2018).

Upon implantation, the epiblast remodels on the cellular level to form an epithelium (Bedzhov and Zernicka-Goetz, 2014; Wallingford et al., 2013). This remodelling and parallel cell polarisation is dependent on extracellular matrix (ECM) components. Upon blastocyst formation at E3.5, the mural TE begins to deposit ECM components along its basal side giving rise to the Reichert's membrane. At E4.5, this membrane consists of thick, multi-layered ECM forming a continuous structure with a second basement membrane established predominantly by the primitive endoderm and deposited between this tissue and the epiblast (Salamat et al., 1995). Formation of both membranes is critical for embryo survival (Miner, 2004; Smyth et al., 1999) and epiblast morphogenesis (Bedzhov and Zernicka-Goetz, 2014; Fassler and Meyer, 1995).

However, whether and how the ECM could affect the acquisition of tissue shape during the implantation stages is currently unknown.

Here, we studied the tissue remodelling events that drive peri-implantation morphogenesis of the epiblast in mouse and human embryos. We found that acquisition of the characteristic cup-shape in mice is determined by increasing contractility and tension in the polar TE, which generates a physical force to push the epiblast into its post-implantation configuration. The polar TE of human embryos acts in the opposite way, exerting a stretching force on the epiblast leading it to adopt a disc-like structure. The polar TE therefore appears to be an evolutionary conserved regulator of epiblast shape upon implantation.

Results

The steps of mouse embryogenesis during the blastocyst to egg cylinder transition

During the transition from pre to post implantation, the mouse epiblast transforms from an oval to a cup-shaped morphology (Figure 1A). To investigate the mechanism underlying this transition, we first carried out a quantitative analysis of epiblast shape at consecutive timepoints from implantation to egg cylinder formation. We found that the epiblast progressed through 5 distinct states (Figure 1B). Initially, it exhibited an oval shape with its long axis parallel to the polar TE, which formed a thin layer of squamous cells (Figure 1C, Stage I). However, 6h following the initiation of implantation, the epiblast became spherical, doubling its total height but retaining a constant width (Figure 1D-G, stage I-II, Figure S1A-B). During the same time period, the polar TE increased in height (Figure 1C, stage II, Figure 1H stage I-II). Strikingly, the epiblast continued to grow in height but not in width during the next 5h of development until it acquired a highly angled rhomboid shape (Figure 1C-G, Figure S1A-B, stage III) while the polar TE increased further in height (Figure 1H, stage II-III). The next developmental stage was characterised 5h later by a pronounced rearrangement of the epiblast from the rhomboid to a cup shape whereupon it came to share a straight tissue interface with the polar TE, which generated a dome-like structure on top of the epiblast (Figure 1C, stage IV). During this rearrangement, the epiblast remained constant in both height and width (Figure 1E,F, stage III-IV) but exhibited continuous growth in total area while retaining a spherical shape (Figure 1G, Figure S1B, stage III-IV). In contrast, the polar TE continued to increase exponentially in height (Figure 1H, stage III-IV). The embryo completed its transformation 1-2h following cup-shape acquisition by folding of the polar TE through apical constriction (Christodoulou et al., 2019) and the epiblast fully acquiring its cup shape giving rise to the post-implantation egg cylinder (Figure 1C, stage V). Subsequently, the epiblast gradually lost its spherical shape to become more cuboid (Figure 1 D-G, Figure S1B, stage IV-V). To understand whether these shape changes in the different lineages could be accounted for by localised cell division or death, we determined the distribution of phospho-Histone 3 and cleaved Caspase 3, respectively (Figure S1C,D) and quantified the cell numbers (Figure S1E,F). Both lineages exhibited a parallel increase in cell number throughout the implantation period, but we could not observe any specific localised cell proliferation or death (Figure S1C,D,

Figure 1I). These results indicate that the epiblast and the polar TE undergo dynamic remodelling after implantation with the epiblast evolving through several distinct spatial configurations before reaching cup shape, which cannot be accounted for by localised tissue proliferation or cell death.

The epiblast and polar trophectoderm interface remodels during blastocyst to egg cylinder transition

To investigate whether the remodelling of the epiblast and polar TE were interconnected, we focussed on the tissue interface (Figure 2A, Figure S2A) and quantified total length, diameter and curvature angle (Figure 2B). Upon implantation, the proximal side the oval epiblast was covered by the polar TE (Figure 2A, stage I Figure S2A, stage I). Length, diameter and the total curvature of the interface increased from stage I to stage II (Figure 2C-E, stage I-II). However, when the epiblast acquired a rhomboid shape (stage III), both interface length and diameter dropped while the curvature remained, suggesting an increase in relative curvature as the interface had become smaller (Figure 2C-E, stage II-III). Concurrent with the remodelling of the epiblast into the cup, the polar TE-epiblast interface transformed from being highly curved into a straight line (Figure 2A-E stage III-IV), indicating that the major tissue rearrangement takes place between stage III and stage IV. At stage V, the interface curvature decreased further to almost 180° (Figure 2C-E, stage V). At the same time, the relative interface (interface diameter/interface total length) approached 1 (Figure 2F). Consequently, we found that the polar TE covered 50% of the epiblast at stages I-II, which decreased to 25% after cup-shape acquisition (stages IV-V) (Figure 2G) while increasing exponentially in aspect ratio (Figure S2B). Together, this suggests that the epiblast minimises its surface presented to the polar TE during egg cylinder formation in a transition from a highly curved to a flat interface.

Alongside tissue architecture changes, the transition from pre- to post-implantation is marked by the epiblast exiting the naïve towards the primed pluripotent state (Nichols and Smith, 2009). To correlate the pluripotency state to the tissue shape changes, we analysed the expression of markers for the naïve state, Nanog, and the primed state, Otx2. Nanog expression became downregulated during stage I, which we therefore further subdivided to represent embryos just prior to implantation and those that initiated implantation based on the morphology of their mural TE. Before implantation, embryos exhibited high levels of Nanog in all epiblast cells and no expression of the Otx2. Upon implantation, 50% of epiblasts showed upregulation of Otx2 and downregulation of Nanog. Nanog expression was completely abolished by stage II (Figure 2H,I, Figure S2 C,D), indicating that exit from naïve pluripotency is completed prior to epiblast remodelling. To correlate tissue shape changes to polarisation on the single cell level, we analysed the localisation of the apical marker Podxl. Podxl was expressed as early as stage II in non-focal patches that became localised to focal points by stage

III and coalesced into a single lumen by stage IV-V (Figure S2E). This illustrates that the progression of epiblast polarisation takes place in parallel to tissue remodelling but does not precede it.

The polar trophoctoderm drives remodelling of the epiblast

To correlate tissue interface changes with the remodelling of the polar TE, we analysed the total curvature and the interface length in relation to the polar TE aspect ratio (polar TE height/total interface length). We found strong correlations for both total curvature and interface length with the polar TE aspect ratio from stage II-V (Figure 3A/B) whereas from stage I-II, embryos exhibited no such correlation or even the opposite trend (Figure S3A,B). These observations suggest that the polar TE is the first tissue to be remodelled and therefore we hypothesised that its remodelling might be driving the shape changes in the epiblast.

To test this, we removed the TE by immuno-surgery incubating implanting blastocysts in anti-mouse serum and then complement serum. The TE was removed through pipetting and embryos were placed in hanging drops of medium to prevent attachment to the dish and so avoid epiblast deformation (Figure S3C, Figure 3C). The epiblast of embryos lacking the TE failed to remodel into a cup and displayed a symmetrical, circular shape (Figure 3D) in contrast to embryos from the control group, which became cup shaped. To confirm that both manipulated embryos and controls exited naïve pluripotency, we analysed the expression of Otx2. Both groups showed high Otx2 expression and had a re-arranged monolayered epithelium surrounding a single constriction point, thus had successfully exited the naïve state. These results suggest that the polar TE is required for the epiblast shape transition.

To gain further insight on whether epiblast remodelling is dependent on the TE and not an inherent capacity of the epiblast, we utilised mouse Embryonic Stem Cells (mESCs) to model the developing epiblast *in vitro* (Bedzhov and Zernicka-Goetz, 2014). We cultured mESCs in differentiating conditions in 3D matrigel and found that after 48h of culture the structures had become spherical, polarised around a focal lumen and upregulated Otx2 expression (Figure 3E-F), in contrast to intact embryos. Even though few outliers exhibited low circularity, none acquired a cup-shape (Figure S3D). These results suggest that cup-shape acquisition is not an inherent capacity of the epiblast during its differentiation process but that it depends on interaction with the polar TE (Figure 3G).

Differential deposition of the extracellular matrix may underline cup shape acquisition

Our initial observation that epiblast width remains constant through remodelling led us to hypothesise that its horizontal expansion, perpendicular to the proximo-distal axis of the embryo, was restricted (Figure 1F). A potential, spatially-restrictive scaffold could be introduced by the ECM as deletion of laminin, one of the main

components of the ECM, leads to a failure of egg cylinder formation (Miner, 2004; Smyth et al., 1999). We therefore decided to investigate the distribution of laminin, as an ECM marker, at implantation.

Initially, laminin was localised peri-cellularly within the primitive endoderm but had not yet formed a continuous basement membrane (BM) along the distal tip of the epiblast (Figure 4A,B). At the same time, the ECM at the border of the Reichert's membrane constituted a thick ring-structure around the epiblast. In the following stages, a thin laminin-positive BM was established between epiblast and primitive endoderm, while the border to the Reichert's membrane continued to show the highest intensity of laminin deposition. Following egg cylinder formation, BM uniformly surrounded the epiblast. Quantitative analysis of laminin localisation revealed a continuous and highly significant increase in the intensity ratio of the BM relative to the border to Reichert's membrane from stage I-III, which stayed constant during the following stages (Figure 4C-D). This result led us to the hypothesis that the edge of Reichert's membrane could introduce spatial constraint toward the epiblast, which would prohibit horizontal growth and movement of the epiblast but not vertical. To understand whether the maturation of the BM into a continuous layer could introduce a similar restriction vertically, we analysed the distance through which the epiblast becomes pushed into the blastocoelic cavity (Figure S4A). Even though a continuous layer of ECM became established, the pushing distance continuously increased; suggesting that the thin BM may not be able to exert a similar restrictive force as Reichert's membrane (Figure 4E). These results suggest that the edge of Reichert's membrane could establish a tight ring around the epiblast prohibiting horizontal growth leading to cup shape acquisition.

Polar trophectoderm tension increases during epiblast remodelling

The dynamic behaviour of the tissue interface between both lineages led us to hypothesise that differential tissue tension and contractility could result in the mechanical force required to drive the epiblast into its cup shape. To establish whether this could be the case, we examined the localisation and total tissue expression levels of E-Cadherin, F-Actin, phosphorylated non-muscle myosin II (pMyosin-II) and Integrin β 1 (Ciobanasu et al., 2013; Sun et al., 2016), as a read-out for tissue contractility and tension (Figure 5A-C, Figure S5A) in embryos at consecutive stages upon implantation and measured the total intensity in epiblast versus polar trophectoderm (Figure 5D). Strikingly, we found that E-Cadherin, F-Actin, Integrin β 1 and pMyosin-II showed similar tissue intensities in the polar TE and the epiblast at stage I (Figure 5A-F stage I, Figure S5 A-B stage I). However, during subsequent development, the E-Cadherin levels increased in the polar TE (Figure 5 A,E, stage II). The same was true for F-Actin (Figure 5 B,F, stage II), which became localised specifically to the apical junctions within the polar TE, pMyosin-II (Figure 5C, stage II) and Integrin β 1 (Figure S5 A-B, stage II). This trend continued up to stage IV for E-Cadherin and then became constant (Figure 5 A,E, stage III-IV). F-actin exhibited increasing intensity in the polar TE throughout development (Figure 5 B,F, stage III-V), whereas pMyosin-II levels decreased slightly upon formation of the egg cylinder in the polar TE (Figure 5C, stage III-IV). Integrin β 1 exhibited increasing expression levels in the polar TE until stage III and then remained constant (Figure S5 A-B). These results suggest that contractility and tension increase within the

polar TE compared to the epiblast during early post-implantation morphogenesis and that differential contractility between the epiblast and polar TE could be an underlying reason for cup-shape acquisition.

To enable increase of contractility, F-Actin must be bound to pMyosin-II. We therefore co-stained embryos for F-actin and pMyosin-II and found that these markers became co-localised increasingly at the apical surface of the polar TE and with time spread from being confined to the cell-cell junctions to form a structure reminiscent of supra-cellular actin cables reported in other systems (Galea et al., 2017) (Figure 5 B,C, Figure S5C). As the polar TE appeared to exhibit contraction across the entire surface of the tissue, we hypothesised that a supra-cellular actin network could generate the force required. To act supra-cellularly, actomyosin must be coupled intercellularly by E-Cadherin and therefore we next examined the expression of E-Cadherin, F-Actin and pMyosin-II (Figure 5G, Figure S5D). F-Actin and pMyosin-II both became increasingly concentrated towards apical cell-cell junctions, colocalising with E-Cadherin at stage III. At stage IV, a cohesive structure was formed apically, interlinked by E-Cadherin and pMyosin-II foci. Surface plots of each factor confirmed this observation, showing a co-localisation of all peaks from stage IV onwards (Figure 5 D,H, Figure S5D-E). This localisation pattern supports the possibility that physical force originating from the polar TE governs epiblast cup-shape acquisition. To investigate whether indeed increased tension and contractility in the polar TE could contribute to the regulation of epiblast shape, we treated embryos at E4.5 with Blebbistatin in hanging drops for 20h to prevent pMyosin-II mediated contractility. Control embryos developed a total curvature angle of 122° between the epiblast and the polar TE (Figure 5I-J), whereas in Blebbistatin treated embryos, the total curvature was significantly higher (90°). These results suggest that pMyosin-II mediated contractility in the polar TE leads to shape changes in the epiblast.

Human blastocysts form bilaminar discs upon implantation

To understand if TE behaviour could influence epiblast shape, we next focussed on human embryos, where the polar TE mediates the implantation process (Figure 6A). The epiblast evolves into a bilaminar disc rather than a cup (Hertig et al., 1956). We hypothesised that that this could be due to stretching of the epiblast through the polar TE. To investigate epiblast shape upon implantation, we analysed the embryos of the Carnegie collection that have been obtained through sectioning of uteri (Hertig, 1945; Hertig et al., 1956). Our observations show that human epiblasts initially form an oval shape similar to mouse embryos, but then become disc-like, growing horizontally but not vertically (Figure 6B-D). Since the low embryo numbers of the Carnegie collection do not allow robust quantitative analysis, we analysed a dataset of 58 pre- and post-implantation *in vitro* cultured human embryos (Molè et al., in revision). These analyses revealed that the epiblast followed a similar trend as observed in the Carnegie stages, resulting in the acquisition of a flat oval shape during post-implantation stages (Figure 6E). The epiblast circularity decreased significantly upon attachment with a similar value as in the Carnegie stages (Figure 6C,F). Similarly, we observed horizontal

growth of the epiblast upon implantation in parallel with our observations from the Carnegie stages (Figure 6D,G).

As contractile tension appears to drive epiblast remodelling in mouse embryos, we hypothesised that loss of such tension would lead mouse embryos to acquire the disc-like shape of human embryos. To test this, we cultured E4.5 mouse embryos for 20h with the Rock inhibitor Y27632 (treated) or DMSO (control). We found that Rock inhibition led embryos to lose pMyosin-II expression, indicating that the inhibition was successful (Figure S6A) and the epiblast of the treated embryos developed into a flat disc or spread over the primitive endoderm in contrast to control embryos, of which 36% established a cup-like shape by the time of fixation (Figure 6H-I, Figure S6B). Thus, the degree of contractile tension in the TE appears to mediate epiblast shape upon implantation.

Discussion

In this study, we provide a comprehensive analysis of the morphogenetic events that lead to tissue remodelling of the mouse embryo upon implantation. We describe how the epiblast and polar TE change their shape over time and provide evidence that epiblast shape is determined by physical force exerted upon it by the overlying TE. We show that the epiblast does not proliferate locally to change from an oval shape into its characteristic cup-shape by flattening its interface with the polar TE and growing distally into the blastocoelic cavity. Instead, it transits through five distinct stages, starting off as an oval structure, developing into a spherical and then a rhomboid shape, sharing a highly angled interface with the polar TE. Only then, does the EPI transform into a cup (Figure 7A).

It has remained unclear how much impact the exit from naïve pluripotency has upon epiblast shape. Our results show that exit from naïve pluripotency towards the formative state (Smith, 2017), initiated upon implantation is completed prior to remodelling of the epiblast, in accord with previous studies (Acampora et al., 2016; Shahbazi et al., 2017). Formation of the cup shape does not occur autonomously in the epiblast lineage but is induced by the TE. Consequently, removal of this tissue leads the epiblast to become spherical. These results indicate the TE as key regulator of epiblast shape. While we cannot rule out an additional regulatory role of the primitive endoderm, our analysis of the extent to which the epiblast is pushed into the blastocoelic cavity (Figure S4a, Figure 4E) indicates that the primitive endoderm does not prevent epiblast expansion. As such, we conclude that the primitive endoderm is likely to have only minor effects on the epiblast shape.

To understand how the TE exerts force upon the epiblast, we investigated localisation and relative concentrations of actomyosin, E-Cadherin, Integrin β 1 and pMyosin-II, known to exhibit increased intensity in contractile tissues (Ciobanasu et al., 2013; Le Duc et al., 2010; Harris et al., 2014; Heer and Martin, 2017), in the epiblast versus the polar TE. E-Cadherin, F-Actin and pMyosin-II levels continuously increase in the

polar TE. This leads us to the conclusion that increasing tension emanating from the polar TE regulates epiblast shape. Removal of contractility through inhibitor treatment, resulted in embryos exhibiting a significantly higher angled interface with the primitive endoderm. Strikingly, we could observe the formation of a continuous actomyosin structure that is established at stage III in the polar TE. We hypothesise that this structure is a supra-cellular actin network analogous to actin cables described in other systems (Begnaud et al., 2016). This could only be proven through intercellular recoil following laser ablation, but the spherical shape of the embryo at these stages would make such measurements impossible. Since the surface of the polar TE remains highly concave until the supra-cellular actomyosin structure is formed, we hypothesise that tension in the polar TE increases until it reaches a tipping point; up to this point, the growth of the epiblast could exert a higher pressure than the growing tension in the polar TE. As soon as this point is reached, the surface between these two tissues becomes flat because tension in the polar TE and pressure through tissue growth from the epiblast became equal. After reaching this stage, the E-Cadherin levels remain constant. As this acts as a tension sensor and transmitter (Buckley et al., 2014; Lecuit and Yap, 2015), it is possible that the tension then remains constant to prevent further deformation of the epiblast. If the polar TE were to continue to exhibit increase in tension, the tissue interface should become convex.

Epiblast proliferation exerts pressure in every direction. We did not find any indication for localised cell proliferation. However, we were only able to observe vertical but no horizontal growth. This suggests a repressive factor prohibits such growth (Dzamba and DeSimone, 2018). By analysing the deposition pattern of ECM, we found that Reichert's membrane forms a tight ring around the epiblast. This ring could introduce the spatial constraint required for successful acquisition of cup shape. Additional factors may also contribute to the restriction of horizontal growth. We have recently shown that upon implantation, a tissue boundary becomes established between the polar and mural TE (Christodoulou et al., 2019). Tissue boundaries were found to be essential for morphogenesis in various systems (Diaz de la Loza and Thompson, 2017; Fagotto, 2014) and can exert contractile forces similar to those of the supra-cellular actin cables found in wound healing and morphogenesis (Begnaud et al., 2016; Galea et al., 2017; Tipping and Wilson, 2011). But as a cable-like structure at this boundary is only observed from the cup to egg cylinder stage (Christodoulou et al., 2019), it seems unlikely that this boundary exerts sufficient force to restrict the epiblast horizontally. We therefore conclude that Reichert's membrane is likely to be the key regulator of the epiblast's horizontal growth.

Finally, we also investigated human epiblast morphogenesis that diverges from the mouse during the implantation stages. In contrast to the mouse, the polar TE of the human embryo mediates implantation and invades the maternal endometrium. This should result in pulling and stretching of the embryo. We therefore analysed embryos that had developed in vivo and were dissected at consecutive stages of peri- and early post implantation development (Hertig et al., 1956; Heuser CH. Rock J. and Hertig AT, 1945) or developing in vitro using a culture method recently established by our lab and others (Deglincerti et al., 2016; Shahbazi et al., 2016). We found that the human embryo does not exhibit any sign of horizontal constraint and develops

into a flat oval, the bilaminar disk. To confirm that polar TE stretching alone could shape the epiblast into a disc structure, we cultured mouse embryos in high concentrations of Rock inhibitor allowing attachment and found that this led to development into flat structures. Even though, Rock inhibition forced the mouse epiblast into a disc-like shape, it is unclear how long the embryo could be maintained in this configuration and whether it could undergo patterning as these developmental steps might be prohibited through off target effects of the Rock inhibitor on epiblast and visceral endoderm lineages. To investigate in detail to what end mouse embryos could mimic human morphology, a tissue specific inducible knock-out of - or overexpression of a dominant negative Rock should be used. Our study provides a precise analysis of tissue shape remodelling upon implantation in the mouse embryo and shows that epiblast shape is dependent on forces exerted by the TE. Moreover, we demonstrate that species-specific remodelling following implantation is likely due to differences in the behaviour of the TE.

Acknowledgements

We are grateful to D. Glover, M.A. Molè, N. Christodoulou, C. Gantner, M. Shahbazi, H. Mudge and E. Paluch for feedback. This study has been enabled through grants from the European Research Council (669198), the Wellcome Trust (098287/Z/12/Z), the EU Horizon 2020 Marie Skłodowska-Curie actions (ImageInLife,721537) and Open Philanthropy and Weston Haven grants at Caltech.

Author Contributions

A.W. and M.Z.G. conceived of and conceptualised the project. A.W. designed and carried out all experiments and data analysis. A.W. and M.Z.G. wrote the manuscript.

Declaration of interests

The authors declare no competing interests.

References

- Acampora, D., Omodei, D., Petrosino, G., Garofalo, A., Savarese, M., Nigro, V., Di Giovannantonio, L.G., Mercadante, V., and Simeone, A. (2016). Loss of the Otx2-Binding Site in the Nanog Promoter Affects the Integrity of Embryonic Stem Cell Subtypes and Specification of Inner Cell Mass-Derived Epiblast. *Cell Rep.* *15*, 2651–2664.
- Bedzhov, I., and Zernicka-Goetz, M. (2014). Self-Organizing Properties of Mouse Pluripotent Cells Initiate Morphogenesis upon Implantation. *Cell* *156*, 1032–1044.
- Begnaud, S., Chen, T., Delacour, D., Mège, R.-M., and Ladoux, B. (2016). Mechanics of epithelial tissues during gap closure. *Curr. Opin. Cell Biol.* *42*, 52–62.
- Buckley, C.D., Tan, J., Anderson, K.L., Hanein, D., Volkmann, N., Weis, W.I., Nelson, W.J., and Dunn, A.R. (2014). The minimal cadherin-catenin complex binds to actin filaments under force. *Science* (80-.). *346*, 1254211–1254211.
- Cartagena-Rivera, A.X., Logue, J.S., Waterman, C.M., and Chadwick, R.S. (2016). Actomyosin Cortical Mechanical Properties in Nonadherent Cells Determined by Atomic Force Microscopy. *Biophys. J.* *110*, 2528–2539.
- Christodoulou, N., Weberling, A., Strathdee, D., Timpson, P., Zernicka-goetz, M., and Anderson, K.I. (2019). Morphogenesis of extra-embryonic tissues directs the remodelling of the mouse embryo at implantation. *Nat. Commun.* 1–12.
- Chugh, P., Clark, A.G., Smith, M.B., Cassani, D.A.D., Dierkes, K., Ragab, A., Roux, P.P., Charras, G., Salbreux, G., and Paluch, E.K. (2017). Actin cortex architecture regulates cell surface tension. *Nat. Cell Biol.* *19*, 689–697.
- Ciobanasu, C., Faivre, B., and Le Clainche, C. (2013). Integrating actin dynamics, mechanotransduction and integrin activation: The multiple functions of actin binding proteins in focal adhesions. *Eur. J. Cell Biol.* *92*, 339–348.
- Copp, A.J. (1978). Interaction between inner cell mass and trophectoderm of the mouse blastocyst. I. A study of cellular proliferation. *J. Embryol. Exp. Morphol.* *48*, 109–125.
- Copp, A.J. (1979). Interaction between inner cell mass and trophectoderm of the mouse blastocyst. II. The fate of the polar trophectoderm. *J. Embryol. Exp. Morphol.* *51*, 109–120.

Deglincerti, A., Croft, G.F., Pietila, L.N., Zernicka-Goetz, M., Siggia, E.D., and Brivanlou, A.H. (2016). Self-organization of the in vitro attached human embryo. *Nature* 533, 251.

Diaz de la Loza, M.C., and Thompson, B.J. (2017). Forces shaping the *Drosophila* wing. *Mech. Dev.* 144, 23–32.

Le Duc, Q., Shi, Q., Blonk, I., Sonnenberg, A., Wang, N., Leckband, D., and De Rooij, J. (2010). Vinculin potentiates E-cadherin mechanosensing and is recruited to actin-anchored sites within adherens junctions in a myosin II-dependent manner. *J. Cell Biol.* 189, 1107–1115.

Dzamba, B.J., and DeSimone, D.W. (2018). Extracellular Matrix (ECM) and the Sculpting of Embryonic Tissues. pp. 245–274.

Fagotto, F. (2014). The cellular basis of tissue separation. *Development* 141, 3303–3318.

Fassler, R., and Meyer, M. (1995). Consequences of lack of beta 1 integrin gene expression in mice. *Genes Dev.* 9, 1896–1908.

Galea, G.L., Cho, Y.-J., Galea, G., Molè, M.A., Rolo, A., Savery, D., Moulding, D., Culshaw, L.H., Nikolopoulou, E., Greene, N.D.E., et al. (2017). Biomechanical coupling facilitates spinal neural tube closure in mouse embryos. *Proc. Natl. Acad. Sci. U. S. A.* 114, E5177–E5186.

Harris, A.R., Daeden, A., and Charras, G.T. (2014). Formation of adherens junctions leads to the emergence of a tissue-level tension in epithelial monolayers. *J. Cell Sci.* 127, 2507–2517.

Heer, N.C., and Martin, A.C. (2017). Tension, contraction and tissue morphogenesis. *Development* 144, 4249–4260.

Hertig, A.T. (1945). On the development of the amnion and exocoelomic membrane in the previllous human ovum. *Yale J. Biol. Med.* 18, 107–115.

Hertig, A.T., Rock, J., and Adams, E.C. (1956). A description of 34 human ova within the first 17 days of development. *Am. J. Anat.* 98, 435–493.

Heuser CH, Rock J. and Hertig AT (1945). Two human embryos showing early stages of the definitive yolk sac. *Contrib. Embryol., Carnegie Inst. Wash. Publ.* 557, 85–99.

Lecuit, T., and Yap, A.S. (2015). E-cadherin junctions as active mechanical integrators in tissue dynamics. *Nat. Cell Biol.* 17, 533–539.

Ma, H., Zhai, J., Wan, H., Jiang, X., Wang, X., Wang, L., Xiang, Y., He, X., Zhao, Z.-A., Zhao, B., et al. (2019). In vitro culture of cynomolgus monkey embryos beyond early gastrulation. *Science* (80-.). 366, eaax7890.

Martin, A.C., Gelbart, M., Fernandez-Gonzalez, R., Kaschube, M., and Wieschaus, E.F. (2010). Integration of contractile forces during tissue invagination. *J. Cell Biol.* 188, 735–749.

Miner, J.H. (2004). Compositional and structural requirements for laminin and basement membranes during mouse embryo implantation and gastrulation. *Development* 131, 2247–2256.

Molè, M.A., Weberling, A., and Zernicka-Goetz, M. (2020). Comparative analysis of human and mouse development: From zygote to pre-gastrulation. pp. 113–138.

Nelson, W.J. (2008). Regulation of cell–cell adhesion by the cadherin–catenin complex. *Biochem. Soc. Trans.* 36, 149–155.

Nichols, J., and Smith, A. (2009). Naive and Primed Pluripotent States. *Cell Stem Cell* 4, 487–492.

Pinheiro, D., and Bellaïche, Y. (2018). Mechanical Force-Driven Adherens Junction Remodeling and Epithelial Dynamics. *Dev. Cell* 47, 3–19.

Salamat, M., Miosge, N., and Herken, R. (1995). Development of Reichert's membrane in the early mouse embryo. *Anat. Embryol. (Berl)*. 192.

Shahbazi, M.N., Jedrusik, A., Vuoristo, S., Recher, G., Hupalowska, A., Bolton, V., Fogarty, N.N.M., Campbell, A., Devito, L., Ilic, D., et al. (2016). Self-organization of the human embryo in the absence of maternal tissues. *Nat. Cell Biol.* 18, 700–708.

Shahbazi, M.N., Scialdone, A., Skorupska, N., Weberling, A., Recher, G., Zhu, M., Jedrusik, A., Devito, L.G., Noli, L., Macaulay, I.C., et al. (2017). Pluripotent state transitions coordinate morphogenesis in mouse and human embryos. *Nature* 552, 239–243.

Smith, A. (2017). Formative pluripotency: the executive phase in a developmental continuum. *Development* 144, 365–373.

Smith, L.J. (1980). Embryonic axis orientation in the mouse and its correlation with blastocyst relationships to the uterus. Part 1. Relationships between 82 hours and 4 1/4 days. *J. Embryol. Exp. Morphol.* 55, 257–277.

Smyth, N., Vatansever, H.S., Murray, P., Meyer, M., Frie, C., Paulsson, M., and Edgar, D. (1999).

Absence of Basement Membranes after Targeting the LAMC1 Gene Results in Embryonic Lethality Due to Failure of Endoderm Differentiation. *J. Cell Biol.* 144, 151–160.

Solter, D., and Knowles, B.B. (1975). Immunosurgery of mouse blastocyst. *Proc. Natl. Acad. Sci.* 72, 5099–5102.

Sun, Z., Guo, S.S., and Fässler, R. (2016). Integrin-mediated mechanotransduction. *J. Cell Biol.* 215, 445–456.

Svitkina, T.M. (2020). Actin Cell Cortex: Structure and Molecular Organization. *Trends Cell Biol.*

Tipping, N., and Wilson, D. (2011). Chick Amniogenesis is Mediated by an Actin Cable. *Anat. Rec. Adv. Integr. Anat. Evol. Biol.* 294, 1143–1149.

Wallingford, M.C., Angelo, J.R., and Mager, J. (2013). Morphogenetic analysis of peri-implantation development. *Dev. Dyn.* 242, 1110–1120.

Yamada, S., Pokutta, S., Drees, F., Weis, W.I., and Nelson, W.J. (2005). Deconstructing the Cadherin-Catenin-Actin Complex. *Cell* 123, 889–901.

Figures

Figure 1. Sequence of remodelling steps of epiblast and polar trophoblast tissues upon implantation. **a.** E4.5 implanting blastocyst and E5.0 early egg cylinder DAPI (blue), F-Actin (green), Oct4 (red). Oct4 is expressed in the epiblast tissue. Zoom in on the epiblast tissue to highlight shapes of the epiblast upon implantation (oval) and post-implantation (cup). **b.** Schematic of the epiblast (pink) and polar TE (blue) lineages from implantation to egg cylinder formation. **c.** Lineage staining of embryos fixed at sequential timepoints from implantation to egg cylinder formation (E4.5-5.0). Top Row: Embryos stained for Gata6 (white) and Cdx2 (blue) to distinguish primitive endoderm and polar TE lineages respectively, DAPI (red) and F-Actin (green). This allows analysis of epiblast and polar TE tissue shapes. Bottom row: Zoom in on epiblast and polar TE lineages with polar TE highlighted in blue and the epiblast in red. **d.** Schematic to illustrate measurements taken for quantitative analysis. Polar TE in blue, epiblast in pink. Measurements were taken in plane of maximum tissue area for both lineages. epiblast height (white) and width (green) measured through the centre of the epiblast. epiblast area (green dotted line) measured for the maximum area. Polar TE height (red) measured at three points, the average for each embryo was analysed. **e.** Quantification of epiblast height (μm) over time, Scatter plot, Mean \pm SEM. The epiblast height changes significantly over time. N numbers of stages: I: n=69, II n=81, III n=51, IV n=40, V n=43. Analysis: unpaired student's t test stages I-II: $p < 0.0001$, II-III: $p=0.0020$, III-IV: $p=0.3530$, IV-V $p= 0.0059$. **f.** Quantification of epiblast width over time, Scatter plot, Mean \pm SEM. Epiblast width increases slightly. N numbers stage I: n=68, II n=81, III n=51, IV n=40, V n=43. Analysis: unpaired student's t test stages I-II: $p=0.6192$, II-III: $p=0.1559$, III-IV= 0.1523 , IV-V: $p=0.2277$, I-V: $p<0.0001$. **g.** Quantification of epiblast area over time. Scatter plot, Mean \pm SEM. Area increases significantly over time. N numbers stage I: n=69, II n=81, III n=51, IV n=40, V n=44. Analysis: unpaired student's t test stages I-II: $p<0.0001$, II-III: $p < 0.0001$, III-IV= 0.0005 , IV-V: $p= 0.4385$. **h.** Quantification of polar TE height over time. Scatter plot, Mean \pm SEM. Height of polar TE increases exponentially over time. N numbers stage I: n=69, II n=82, III n=51, IV n=40, V n=44. Analysis: unpaired student's t test. Stages I-II: $p<0.0001$, II-III: $p<0.0001$, III-IV <0.0001 , IV-V: $p<0.0001$. Scale bars = $20\mu\text{m}$. **i.** Analysis of epiblast and polar TE cell number over time. Stages I: black, II: red, III: yellow, IV: blue, V: green. The growth in cell numbers is highly correlated Pearson $r= 0.8884$, $p<0.0001$, N numbers stages I = 62, II = 51, III = 16, IV = 17, V = 28.

Figure 2. The dynamics of the tissue interface suggest force transmission of the polar trophoblast towards the epiblast. **a.** Lineage staining of embryos fixed at consecutive timepoints from implantation to egg cylinder formation. Staining: DAPI (blue), Gata6 (white), Cdx2 (blue) and F-Actin (green). Tissue interface between epiblast and polar TE defined through F-Actin (white dotted line). **b.** Schematic of quantifications carried out. Polar TE (blue) and epiblast (pink). Interface was analysed for the following parameters: Total length of interface (green dotted line), Interface diameter (blue) and total curvature angle (white). **c.** Quantitative analysis of tissue interface length over time. Scatter plot, Mean \pm SEM. Interface length increased, then dropped significantly. N numbers stage I n=68, II n=81, III n=51, IV n=40, V n=44. Analysis:

unpaired student's t test. Stages I-II: $p < 0.0001$, II-III: $p = 0.0081$, III-IV < 0.0001 , IV-V: $p = 0.5749$. **d.** Quantitative analysis of diameter of tissue interface over time. Scatter plot, Mean \pm SEM. Diameter increased and then decreased to a steady state. N numbers stage I $n = 68$, II $n = 81$, III $n = 51$, IV $n = 40$, V $n = 44$. Analysis: unpaired student's t test. Stages I-II: $p < 0.0001$, II-III: $p = 0.0014$, III-IV < 0.0001 , IV-V: $p = 0.4693$. **e.** Quantitative Analysis of the total Curvature of interface. Scatter plot, Mean \pm SEM. Curvature first dropped to then vastly increase going against 180° . N numbers stages I $n = 68$, II $n = 81$, III $n = 51$, IV $n = 40$, V $n = 44$. Analysis: unpaired student's t test stages: I-II: $p = 0.0152$, II-III: $p = 0.5655$, III-IV < 0.0001 , IV-V: $p = 0.0136$. **f.** Quantitative Analysis of the relative Interface (total length/diameter) over time. Scatter plot, Mean \pm SEM. Relative interface first increased from ~ 1.4 to ~ 1.45 to then go against 1. N numbers as in (c). Analysis: unpaired student's t test stages: I-II: $p = 0.0229$, II-III: $p = 0.7226$, III-IV < 0.0001 , IV-V: $p = 0.0005$. **g.** Quantitative analysis of epiblast coverage by the polar TE (total perimeter/length of interface) over time. Scatter plot, Mean \pm SEM. EPIBLAST was covered up to 50% by polar TE, this decreased to about 25% after cup formation. N numbers stage I $n = 68$, II $n = 81$, III $n = 51$, IV $n = 40$, V $n = 44$. Analysis: unpaired student's t test stages I-II: $p = 0.1128$, II-III: $p < 0.0001$, III-IV < 0.0001 , IV-V: $p = 0.6305$. **h.** Staining of exit from naïve pluripotency over time. Nanog (red) expressed only at stage I, primed pluripotency marker, Otx2 (blue) from stage I onwards and then steadily upregulated. F-Actin (green) allows staging of the embryos. **i.** Quantitative analysis of expression dynamics of Nanog and Otx2. Mean gray value measured at 3 different z-positions per embryo. Mean of the ratio Nanog/Otx2 plotted. Nanog expression was lost already during stage I. N numbers stage Ia=21, Ib=18, II=14, III=13, IV=3. Scatter plot, Mean \pm SEM. Analysis unpaired student's t test stages Ia-Ib: $p < 0.0001$, Ib-II: $p = 0.0015$, II-III: $p = 0.1120$, III-IV: $p = 0.7389$.

Figure 3. The polar trophectoderm induces cup shape formation of the epiblast. **a.** Correlation analysis of polar TE aspect ratio (total height/length of interface) with curvature. Stage II-V had a strong positive correlation. N numbers stage I=68, II=81, III=51, IV=40, stage V=44. Analysis: $r = 0.7414$, $p < 0.0001$. stage I: black, stage II: red, stage III: yellow, stage IV: blue, stage V: green. **b.** Correlation analysis of polar TE aspect ratio with the length of the tissue interface. Strong anti-correlation of stages II-V. N numbers stage I=68, stage II=81, III=51, IV=40, V=44. Analysis: $r = -0.7572$, $p < 0.0001$. **c.** Staining of E4.5 embryo cultured for 48h in hanging drops following immuno-surgery (2 left columns) and control (right column). Embryos stained for DAPI red, F-Actin green and HNF4alpha blue, top row. Otx2 in bottom row. **d.** Quantification of the circularity of the epiblast following immuno-surgery and hanging drop culture. For treated embryos (IS) only those were analysed, where the full TE tissue could be removed. For Controls (Ctrl), only embryos were considered, which retained all three lineages. N(treated)=6, N(control)=4. Scatter plot, Mean \pm SEM **e.** mouse embryonic stem cells (mESCs) cultured for 48h in 3D Matrigel in differentiating conditions. Structures stained for DAPI (red), F-Actin (green), Otx2 (white). **f.** Quantitative analysis of the circularity of mESC structures. N=40. Scatter plot, Mean \pm SEM. Structures collected from 4 independent experiments. **g.** Model for the hypothetical

forces required to regulate EPIBLAST cup shape acquisition. polar TE (blue), epiblast (magenta-purple). All scale bars = 20 μ m.

Figure 4. The ECM shows a clear distribution upon implantation. **a.** Expression of laminin upon implantation from stage I-V. Fire-staining represents intensity of signal with purple being low and yellow showing high intensity. **b.** Intensity profiles of laminin signal from (a). BM traced by spline fit, line width of 5 μ m. **c.** Schematic for intensity quantification of Laminin expression. Mean gray value of BM (green) determined through tracing by spline fit with a line width of 5 μ m. Mean gray value of the border between BM and Reichert's membrane (red) determined. **d.** Quantitative Analysis of laminin intensity ratio BM versus mean of the border between Reichert's membrane and BM for each embryo. Intensity ratio increases significantly up to stage III, then remains constant. Scatter plot, Mean \pm SEM. N numbers stage I n=59, II n=46, III n=27, IV n=8, V n=33. Analysis unpaired student's t test stages I-II p= 0.0023, II-III p= 0.0002, II-IV p= 0.6952, IV-V p= 0.5181. **e.** Quantification of the pushing distance of the epiblast distal tip towards blastocoelic cavity. Epiblast pushed down continuously with a high significance. Mean \pm SEM. N numbers stages I n=65, II n=81, III n=51, IV n=39, V n=43. Analysis unpaired student's t test stages I-II p<0.0001, II-III p<0.0001, III-IV p<0.0001, IV-V p<0.0001. All scale-bars 20 μ m.

Figure 5. Differential expression of E-Cadherin and F-Actin in polar trophoctoderm and epiblast. **a.** E-Cadherin staining of embryos fixed upon implantation up to egg cylinder formation. Fire-staining represents intensity of signal with purple being lowly and yellow showing highly expressed. **b.** F-actin staining of embryos fixed at consecutive stages from implantation to egg cylinder formation, intensity represented through fire staining (a). A clear increase in the actin intensity from stage I to stage V visible in the polar TE. **c.** pMyosin-II staining of embryos from implantation to egg cylinder formation. Intensity represented through fire staining (a). pMyosin-II exhibits similar staining pattern as F-Actin. **d.** Schematic illustrating the intensity measurements on tissue level (epiblast in magenta-purple, green stripes mark the area of tissue intensity measurement, polar TE in blue, area here marked with white stripes) and level at which plot profiles were taken (red). **e.** Quantitative analysis of the E-Cadherin intensity ratio. For each embryo, the mean gray value of both tissues was determined at 3 different z-positions. The mean of the ratio polar TE/epiblast was plotted. As clearly visible, the polar TE intensity increased significantly over time. Scatter plot, Mean \pm SEM. N numbers stages I n=35, II n=30 III n=19, IV n=24, V n=14. Analysis unpaired student's t test stages I-II p=0.0007, II-III p= 0.0949, II-IV p< 0.0001, IV-V p= 0.5729. **f.** Quantitative analysis of the relative F-actin intensity (polar TE/epiblast) over time averaged for each embryo from measurements of the mean grey value of both tissues at 3 different stages. Scatter plot of average values with Mean \pm SEM. Relative actin intensity clearly increased over time. N numbers of stages: I n=63, II n=65, III n=48, IV n=33, V n=32. Analysis: unpaired student's t test. Stage I-V: p= 0.0100. **g.** Expression analysis of F-Actin (green), pMyosin II (red) and E-Cadherin (blue) in the polar TE from stage I to stage III. White rectangles in the full figures illustrate the region of zoom in. **h.** Merged Plot profiles of the apical surface of the polar TE in (g). A spline fit line was drawn with a thickness of 5 μ m. Plot profile determined through Fiji. F-actin (green), pMyosin-II (red), E-

Cadherin (blue). It is visible that from stage I-IV, the peaks of each marker begin to overlay. **i.** Representative IF stainings of E4.5 embryos cultured for 20h in hanging drop culture supplemented with 100 μ M of Blebbistatin or DMSO in controls. Embryos stained for F-Actin (green), pMyosin II (white), Cdx2 (red), Gata6 (blue), experiment carried out 4x. The shape of the EPIBLAST annotated through a white, dotted line. **j.** Quantitative analysis of the total curvature angle of the tissue interface epiblast/polar TE in treated embryos versus controls. N numbers: control: 12, treated: 11. Analysis: unpaired student's t-test: $p=0.0249$. treated and control embryos differ significantly. All scale-bars 20 μ m.

Figure 6. Human epiblasts are not constricted horizontally upon implantation. **a.** Schematic drawing of a human blastocyst upon implantation at embryonic day (D) 7. Implantation into the maternal endometrium (beige) mediated by the polar TE (blue), overlying the epiblast/inner cell mass (magenta-purple). The implantation results in differentiation and invasion of the trophectoderm/ trophoblast, which is hypothesised to exhibit stretching and pulling forces on the epiblast (red arrows). Following implantation, the epiblast acquires a bilaminar disc-like structure forming a flat oval (D8-9). **b.** Analysis of epiblast shapes of embryos from the Carnegie collection. EPIBLAST highlighted through a red dashed line. Blastocyst: Carnegie embryo 8663; D7.5: Carnegie embryo 8020; D8: Carnegie embryo 8155; D9: Carnegie embryo 8004; D11-12: Carnegie embryo 7700. **c.** Quantitative analysis of epiblast circularity of Carnegie embryos from blastocyst to D11-12. Scatter plot and Mean. **d.** Quantitative analysis of epiblast aspect ratio (height versus width) of Carnegie embryos from blastocyst stage to D11-12. Scatter plot and Mean. **e.** IF staining of in-vitro cultured embryos from D6 to D9. Red: OCT4 (D6-8), OCT4 + PODXL (D9); Blue: DAPI (D6-7,9), AP2 Γ (D8). All scale-bars 20 μ m. **f.** Quantitative analysis of the circularity of in-vitro cultured embryos from D6-D9. The circularity continuously decreases as the epiblast becomes more oval-shaped. Scatter plot, Mean \pm SEM. Analysis unpaired student's t test: D6-D9 $p=0.0042$. D6 n=7, D7 n=10, D8 n=20, D9 n=21. **g.** Quantitative analysis of epiblast aspect ratio (height/width) of in-vitro cultured embryos from (f). Aspect ratio decreases significantly upon implantation. D7-D9 p -value 0.0219 **h.** Y27632 treatment of mouse embryos in attachment culture for 20h. Treated embryos cultured in 100 μ M of Y27632, controls cultured in DMSO. Embryos stained for Oct4 (green), Gata6 (blue), pMyosin II (red) and DAPI (grays). Experiment carried out 3x. Dashed white line encircles epiblast lineage. **i.** Analysis of epiblast coverage angle by the primitive endoderm in Y27632 treated embryos versus controls. The controls are significantly higher covered than the treated embryos, in which the coverage angle in several cases inverted with epiblast spreading over the primitive endoderm instead. Analysis unpaired student's t-test: $p=0.0425$. N numbers: controls: 10, treated: 9.

Figure 7. Model of epiblast remodelling at implantation. **a.** Upon implantation, stage I, the oval-shaped naïve epiblast (magenta-purple) exits from naïve pluripotency towards the primed state (yellow-orange) and increases in area. A thick layer of Reichert's membrane constricts horizontal growth (red arrow heads) leading to the epiblast to only grow vertically (light blue arrows) to adopt a circular shape at stage II. At the same time, the polar TE (dark blue) began to increase in height due to a tissue boundary developed towards the mural trophectoderm (light blue) and begins to exhibit increased levels of tension and contractility (red cell

membranes). Continuous growth of the epiblast in addition to constrictive force of the Reichert's membrane lead to acquisition of a rhomboid shape (stage III). Then, the polar TE begins to constrict apically (long red arrows) exerting force towards the epiblast, transforming the concave surface to a flat disk, which leads the epiblast to become a cup, only able to grow towards the proximal side. Further apical constriction of the polar TE results in formation of the egg cylinder (stage V).

Star Methods

Resource Availability

Lead Contact:

Requests for resources as well as for further information should be directed to and will be fulfilled the lead contact Dr. Magdalena Zernicka-Goetz (mz205@cam.ac.uk)

Materials Availability

This study did not generate new unique reagents.

Data and Code Availability

The original raw dataset of mouse embryo immunofluorescence images and in vitro cultured human embryo immunofluorescence images is available upon reasonable request through the lead contact. The raw data all graphs are based on are found in Table S1.

Experimental Model and Subject Details

Mouse Embryos

The mice used were kept according to national and international guidelines in the animal facility. All experiments carried out have been regulated by the Animals (Scientific Procedures) Act 1986 Amendment Regulations 2012 in addition to ethical review by the University of Cambridge Animal Welfare and Ethical Review Body (AWERB). The Home office has authorised the experiments (License number 70/8864). Mice were culled through cervical dislocation upon any identification of a health concern. Males used in this study were between 6 weeks to 11 months old. The females used in this study were between 6-9 weeks old.

Mouse Embryonic Stem Cells

mESCs were derived directly from mouse embryos and have been generated in the MZG lab.

Method Details

Mouse embryo Recovery

Peri-implantation and early post-implantation stage embryos were dissected from the uteri or deciduas and fixed immediately. Embryos were obtained by crosses of CD1 females with either F1, MF1 or CD1 or endogenous homozygous E-Cadherin-GFP males.

Mouse embryo culture

Embryos were cultured in Advanced IVC medium: CMRL (11530037, Thermo Fisher Scientific) supplemented with 1X B27 (17504001, Thermo Fisher Scientific), 1X N2 (homemade or commercial 17502048, Thermo Fisher Scientific), 1X penicillin–streptomycin (15140122, Thermo Fisher Scientific), 1X GlutaMAX (35050-038, Thermo Fisher Scientific), 1X sodium pyruvate (11360039, Thermo Fisher Scientific), 1X essential amino acids (11130-036, Thermo Fisher Scientific), 1X non-essential amino acids (11140-035,

Thermo Fisher Scientific), 1.8 mM glucose (G8644, Sigma). The medium was developed based on an improved mouse culture system (Ma et al., 2019).

Immuno-surgery and Hanging drop Culture

Immuno-surgery was performed on E4.5 embryos (Solter and Knowles, 1975). Embryos were recovered from mouse uteri and incubated for 15 min in advanced IVC medium supplemented with 20% anti-mouse serum (rabbit, M5774, Sigma Aldrich) for 20 min at 37°C. Following incubation, embryos were washed 3x in advanced IVC medium, placed in IVC medium supplemented with 20% complement (home-made rat serum, gift of Thorsten Boroviak) and incubated for 15 min at 37°C. Embryos were washed for 3x and thereby the trophectoderm lineage, which died through the antiserum and complement incubation, was removed through pipetting. Then, the embryos were placed in hanging drops, 2-2.5 ul of advanced IVC medium supplemented with 30% of FBS and 1ug/ml of Fibronectin (FC010, Sigma Aldrich) for 48h. Hanging drop culture was carried out in order to prevent attachment to the dish and thereby spreading of the epiblast. Each embryo was cultured in a single drop to prevent merging of embryos. After 24h, the embryos were changed to fresh drops.

Inhibitor treatments

Mouse embryos were recovered at E4.5., when implantation was initiated. Following dissection, the mural trophectoderm was removed. For Blebbistatin treatment, the embryos were then cultured for 20h in hanging drops of advanced IVC medium, 30% of FBS and 1ug/ml of Fibronectin (FC010, Sigma Aldrich) supplemented with 100uM of Blebbistatin (B0560, Sigma Aldrich), controls were cultured in DMSO. For Rock inhibition, the embryos were cultured for 20h in advanced IVC medium, 30% of FBS and placed in ibidi dishes to allow attachment (80826, ibidi). Treated embryos were cultured in 100uM of Rock inhibitor Y27632 (72304, Stemcell Technologies), controls were placed in DMSO.

mESC Culture

mESCs were cultured on gelatine (G7765, Sigma Aldrich) in Feeder Cell (FC) medium composed of DMEM (41966, Thermo Fisher Scientific), 15% Fetal Bovine Serum (Stem Cell Institute), 1x penicillin–streptomycin (15140122, Thermo Fisher Scientific), 1x GlutaMAX (35050-038, Thermo Fisher Scientific), 1x non-essential amino acids (11140-035, Thermo Fisher Scientific), 1x sodium pyruvate (11360039, Thermo Fisher Scientific) and 100 µM β-mercaptoethanol (31350-010, Thermo Fisher Scientific), which was supplemented with 2iLIF to preserve naïve pluripotency (1 µM MEK inhibitor PD0325901 (Stem Cell Institute), 3 µM GSK3 inhibitor CHIR99021 (Stem Cell Institute) and 10 ng/ml LIF (Stem Cell Institute). mESC propagation was carried out at 37°C, 5% CO₂ in a humidified atmosphere. Medium was changed every 48h. Passaging was carried out every 48-72h depending on confluency and colony size. For this, the cells were washed with phosphate buffered saline (PBS, 10010056, Life Technologies) and then incubated with TrypLE Express Enzyme (12604-021, Thermo Fisher Scientific) for 3 min at 37°C. The reaction was stopped with an excess of FC medium. The cell suspension was centrifuged at 1.000rpm for 5 min and the cells were resuspended in FC-2iLIF medium and seeded in 1:10 or 1:20 dilution.

Cells were trypsinised, resuspended in 1ml of PBS and counted. 15.000 cells/well were seeded in 20 μ l of ice-cold Matrigel (354230, SLS) in an ibidi-plate (80821, ibidi) and incubated for 5 min at 37°C. then, cells were incubated for 48h in N2B27 medium to allow differentiation. N2B27 medium was composed of 50% DMEM F12 (21331-020, Thermo Fisher Scientific) and 50% of Neurobasal A (10888-022, Thermo Fisher Scientific). This base was supplemented with 1x B27 (17504001, Thermo Fisher Scientific), 1x N2 (homemade or 17502048, Thermo Fisher Scientific), 100 μ M β -mercaptoethanol (31350-010, Thermo Fisher Scientific), 1x penicillin–streptomycin (15140122, Thermo Fisher Scientific) and 1x GlutaMAX (35050-038, Thermo Fisher Scientific).

Embryo Fixation and IF

Embryos transferred to 4% paraformaldehyde (PFA) in phosphate buffered saline (PBS) immediately following recovery and kept on ice. Once recovery was completed, embryos were fixed for additional 20 min at room temperature (RT). All incubation steps were carried out in well coated with filtered fetal bovine serum (FBS) to avoid attachment to the bottom of the wells. mESCs were fixed in 4% PFA in PBS for 25 min at RT. Permeabilisation was carried out through incubation in 0.3% Triton X-100/0.1 M Glycin in PBS for 20 min (Embryos) or 25 min (mESCs). Primary antibody incubation was performed in blocking solution (0.1% Tween-20, 10% FBS, 1% bovine serum albumin (BSA) in PBS) at 4°C overnight. Secondary antibodies and nuclear stain using DAPI (10mg/ml) were prepared simultaneously in blocking solution mixed and centrifuged for 5 min at 14.000rpm. Incubation was carried out for 3h at RT in the dark. Washes were performed in PBS supplemented with 0.1% Tween-20. **Primary antibodies** used: mouse-Oct3/4 (sc-5279, Santa Cruz, 1:200), mouse-Cdx2 (MU392-UC, Biogenex, 1:200), rabbit-Cdx2 (ab76541, Abcam, 1:200), goat-Gata6 (AF1700, R&D, 1:200), rabbit-Nanog (ab80892, Abcam, 1:200), goat-Otx2 (AF1979, R&D Systems, 1:200), rabbit-HNF4 (ab201460, Abcam, 1:1500), rabbit-Laminin (L9393, Sigma Aldrich, 1:300), rat-E-Cadherin (13-1900, Thermo-Fisher, 1:300), rabbit-phosphorylated-Myosin II (3671S, Cell Signalling Technology), rat-GFP (GF090R, Fine Chemical Products Ltd. 1:1000), rat-Podxl (MAB1556, R&D Systems, 1:200), rat Integrin β 1 (MAB1997, Millipore, 1:150), rabbit-cleaved Caspase 3 (9664S, Cell Signalling Technologies, 1:200), rabbit phospho Histone 3 (9701S, Cell Signalling Technologies, 1:1000). **Secondary antibodies** used: Phalloidin-Alexa Fluor (AF) 405 (A30104, Thermo Fisher Scientific 1:250), Phalloidin-AF 488 (A12379, Thermo Fisher Scientific, 1:500), Phalloidin-AF 594 (A12381, Thermo Fisher Scientific, 1:250), AF 568 Donkey-Anti-Rabbit (A10042, Life Technologies, 1:500), AF 568 Donkey-Anti Goat (A-11057, Life Technologies), AF 568 Donkey-anti-Mouse (A10037, Life Technologies, 1:500), AF 647 Donkey-anti-Rabbit (A-31573, Life Technologies, 1:500), AF 647 Donkey-anti-Goat (A21447, Invitrogen, 1:500), AF 488 Donkey-anti-Rat (A-21208, Life Technologies, 1:500).

Imaging, image processing and analysis

Imaging of embryos and mESCs was performed on a Leica SP8 confocal microscope using a 63x-oil objective. Z-stacks were taken at a step size of 0.6 μ m. The images were processed using the Fiji software. Analysis was performed using the Fiji software.

Quantification and Statistical Analysis

For statistical analysis of all quantitative analyses carried out, GraphPad Prism 6.0 was used. The sample size is based on previous experimental experiences. For immuno-surgery, embryos were assigned randomly to either treated or control group, this experiment was carried out 3 times.

For all other quantification, the embryos were collected at least three different dates. Every quantification is shown with single data point clouds in addition to the Mean \pm SEM. Each datapoint represents a single embryo.

For intensity measurements of whole tissues, the mean gray value was obtained at three different z-positions per embryo. The mean was used for further analysis. The statistical tests performed on each quantification are annotated in the figure legend.

Table S1: Raw data of analyses carried out related to Figure 1-6, Figure S1-3,5.

Figure 1

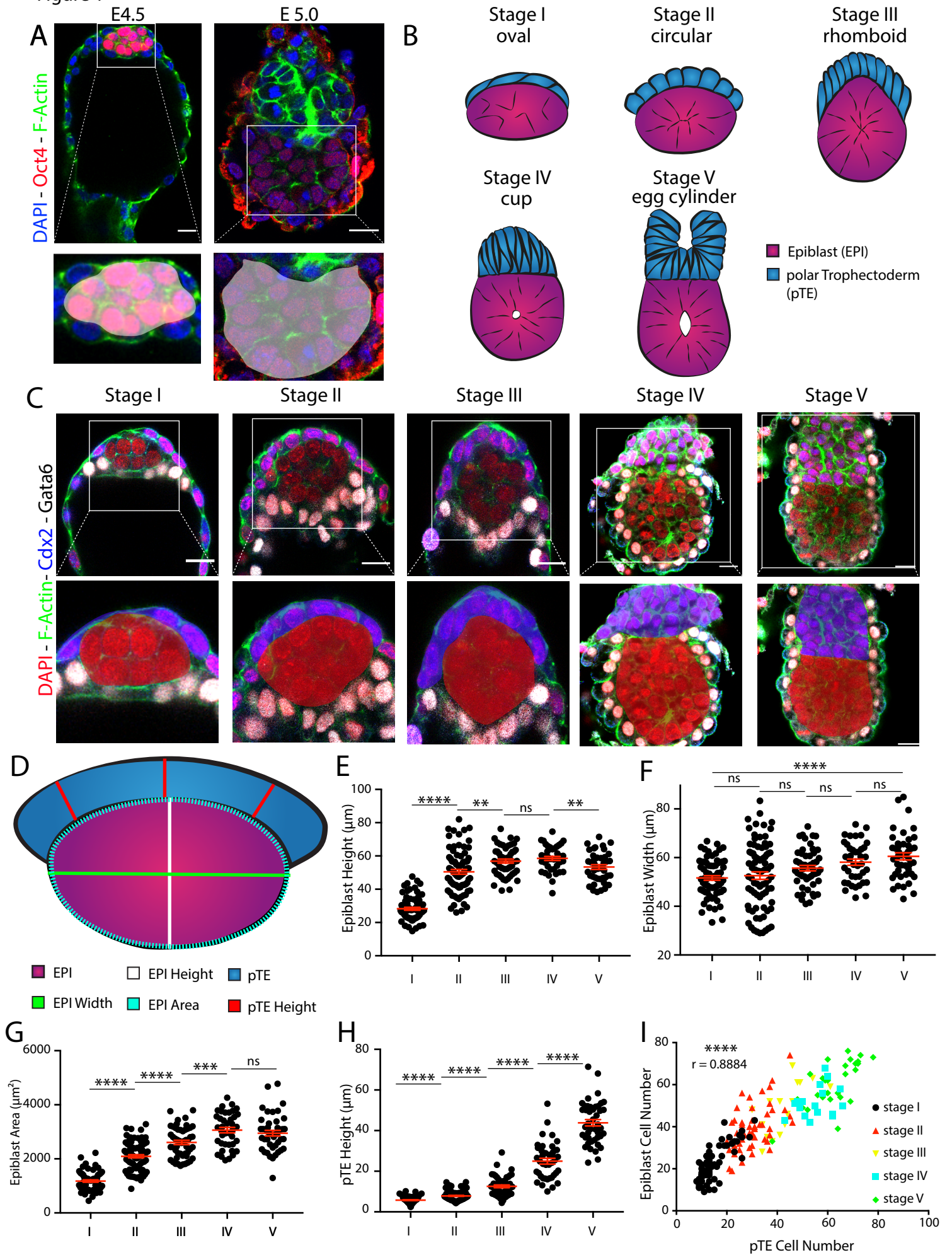


Figure 2

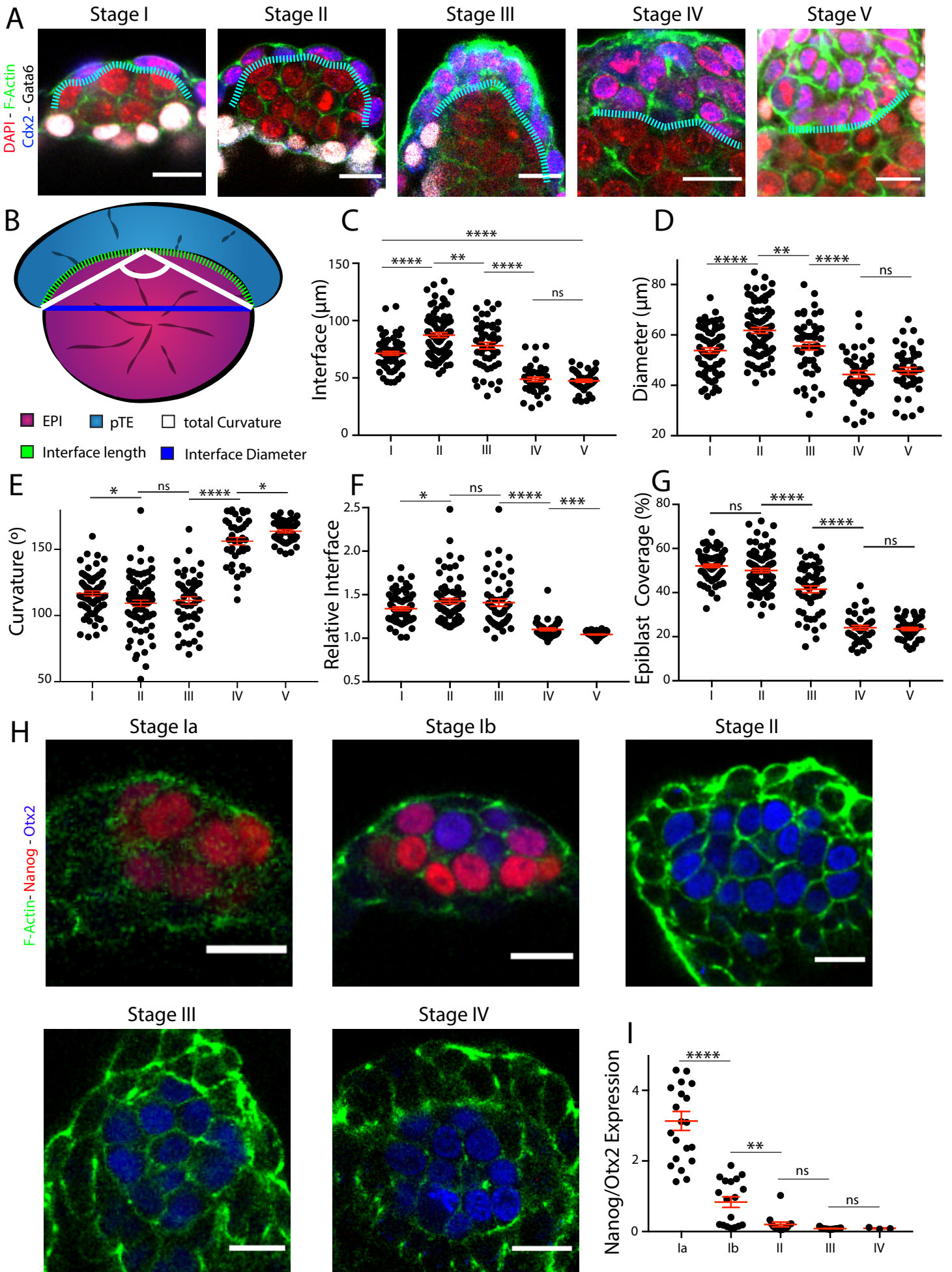


Figure 3

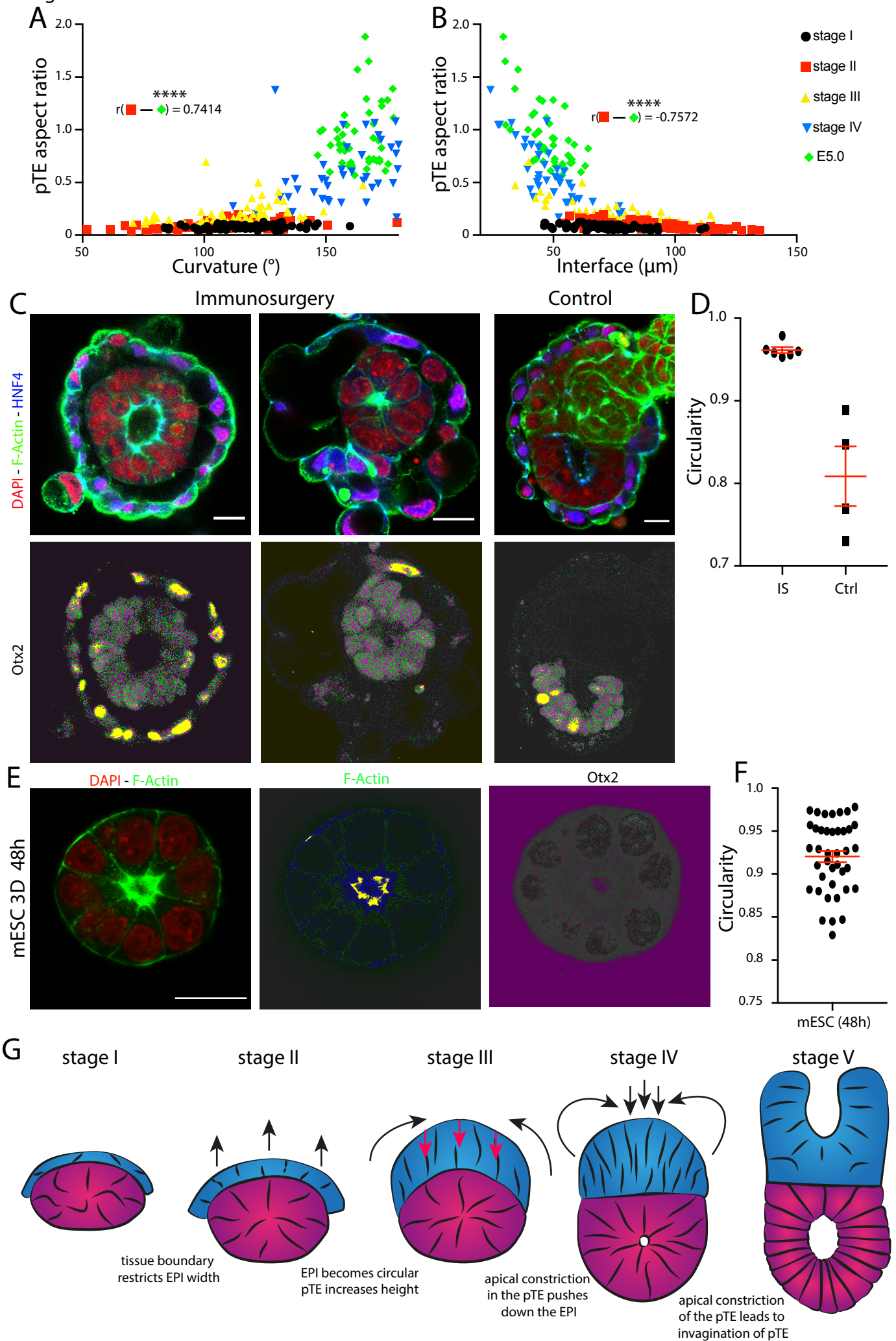


Figure 4

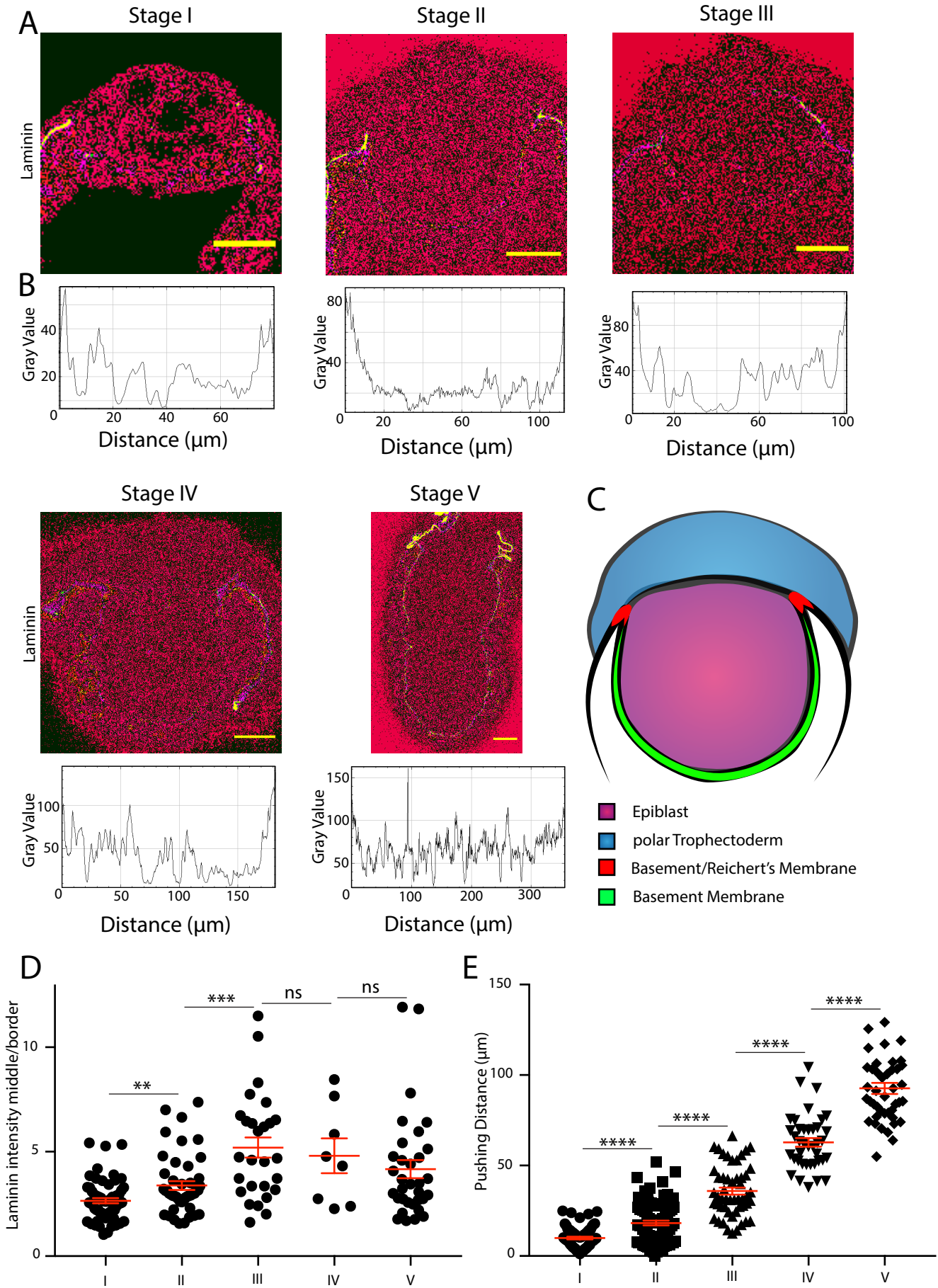


Figure 5

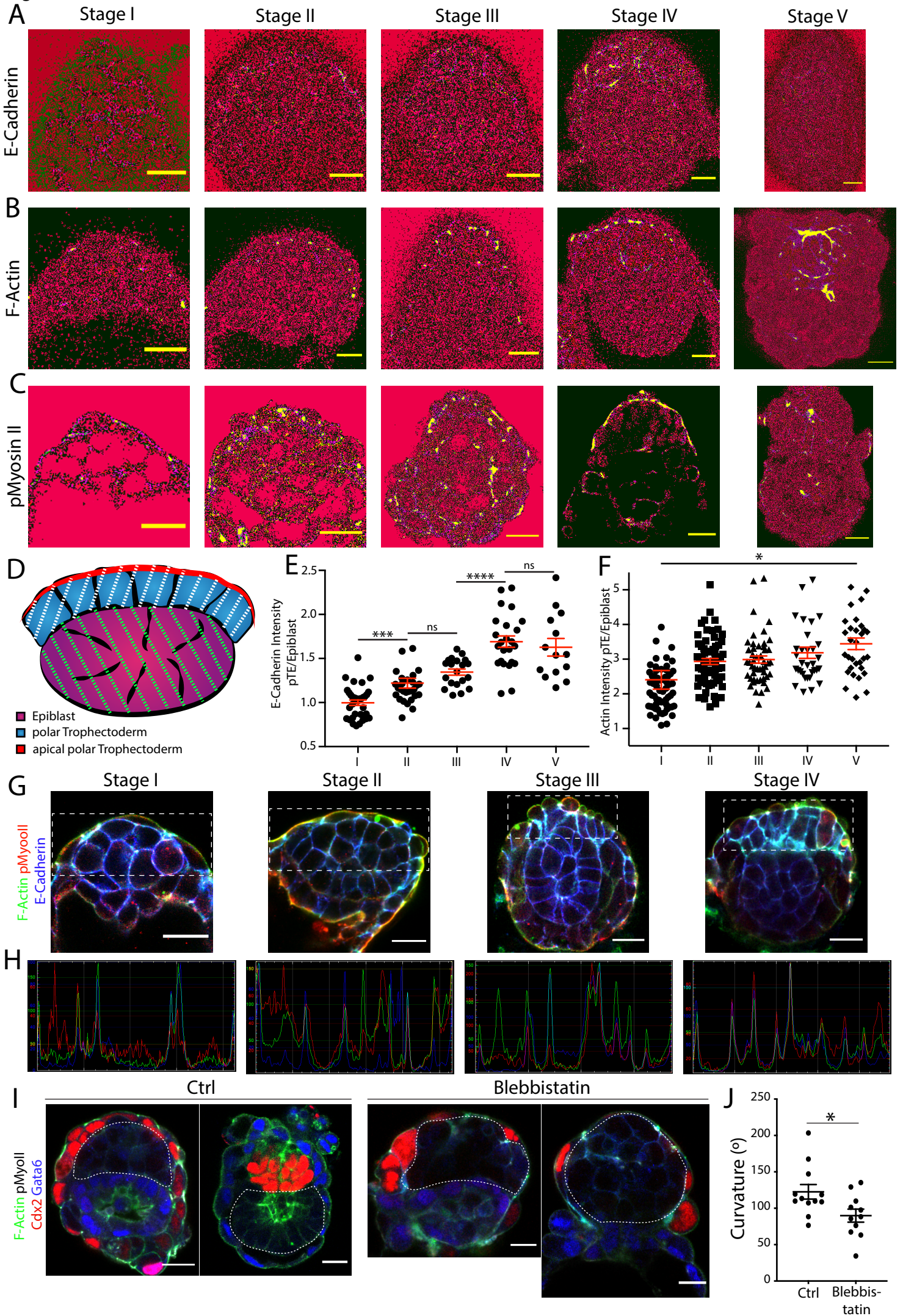


Figure 6

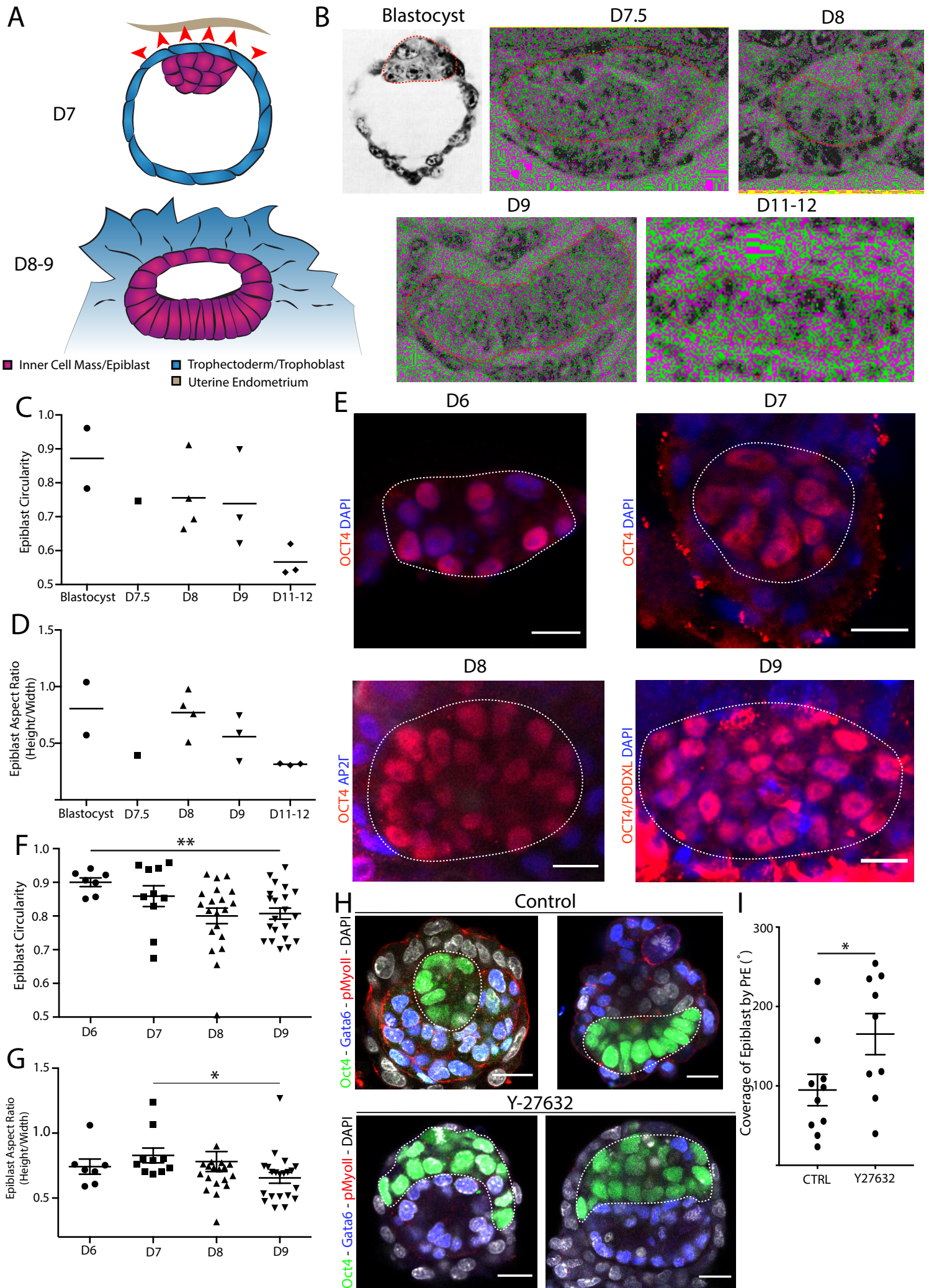
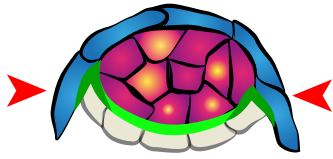


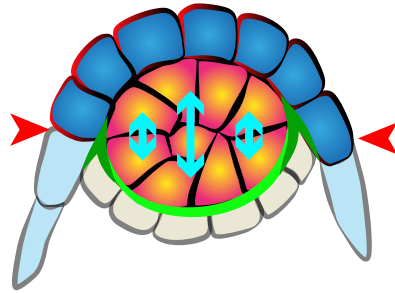
Figure 7

A

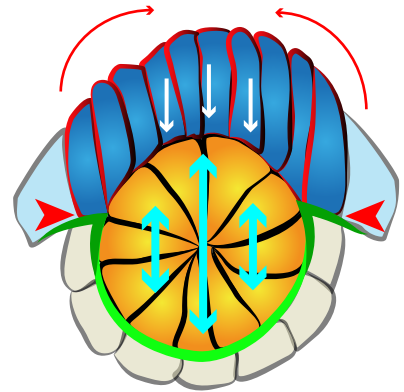
Stage I
oval



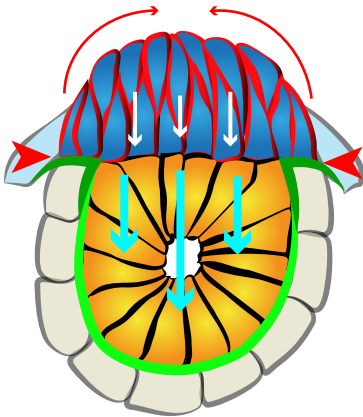
Stage II
round



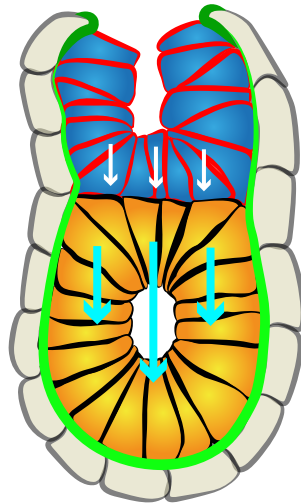
Stage III
rhomboid



Stage IV
cup



Stage V
E5.0



-  polar Trophectoderm/
Extraembryonic Ectoderm
-  naïve Epiblast
-  formative/primed Epiblast
-  primitive Endoderm/
Visceral Endoderm
-  mural Trophectoderm
-  Basement Membrane
-  Reichert's Membrane